Synthesis and characterization of carbon xerogel/graphene hybrids as adsorbents for metronidazole pharmaceutical removal: effect of operating parameters

Sonia Judith Segovia-Sandoval[a], Luisa M. Pastrana-Martínez*[b], Raúl Ocampo-Pérez*[c],

Sergio Morales-Torres [b], María Selene Berber-Mendoza[a], Francisco Carrasco-Marín [b]

[a] *Center of Investigation and Postgraduate Studies, Faculty of Engineering, Autonomous University of San Luis Potosí, Av. Dr. M. Nava No. 6, San Luis Potosí SLP 78210, Mexico.*

[b]*Carbon Materials Research Group, Department of Inorganic Chemistry, Faculty of Sciences, University of Granada, Avenida de Fuentenueva, s/n., ES18071 Granada, Spain.*

[c]*Center of Investigation and Postgraduate Studies, Faculty of Chemical Science, Autonomous University of San Luis Potosí, Av. Dr. M. Nava No. 6, San Luis Potosí SLP 78210, Mexico.*

*Corresponding author e-mail addresses:

raul.ocampo@uaslp.mx (R. Ocampo Pérez)

Tel: 52-4442344709

lpastrana@ugr.es (L. M. Pastrana-Martínez)

Tel: +34-958240443

Fax: +34-958248526

Abstract

In this work, a series of carbon xerogel/graphene hybrids were synthesized from resorcinol and formaldehyde by adding increasing loadings of graphene oxide (GO) solution. Resulting samples were functionalized with urea and characterized by SEM, adsorption-desorption isotherms of N_2 at 77 K, X-ray photoelectron spectroscopy (XPS), and RAMAN spectroscopy. Carbon xerogel/graphene hybrids were assessed as adsorbents for metronidazole (MNZ) removal in aqueous solutions under different operational conditions (solution pH, temperature, ionic strength, and type of water) to determine its adsorption mechanism. The maximum adsorption capacities (q_m) of carbon xerogel/graphene hybrids towards MNZ were in the range of 110-166 mg g^{-1} at pH 5 and 298 K. Moreover, the results showed almost a linear relationship between S_{BET} and q_m. The adsorption capacity of MNZ decreased at ionic strength lower than 0.01 N NaCl and remained constant at higher ionic strength. MNZ adsorption is not inhibited by the presence of ions in treated water and the process exhibited endothermic nature. Based on the obtained results from the adsorption equilibrium, the MNZ removal might occurred by different mechanism such as π-π dispersive interactions, attractive electrostatic interactions (at pH 8), and hydrogen bonds.

1. INTRODUCTION

Antibiotics are extensively used as therapeutic agents in the treatment of human and animal infectious diseases, but nowadays they are also used in livestock industry and aquaculture as feed additives as prophylactics and growth promoters [1]. Antibiotics can be incorporated into the water environment through the effluent and sludge from domestic wastewater treatment plants, hospitals, health care centers, pharmaceutical and agricultural industries, and livestock farms at concentrations generally ranging between 0.01 and 1.0 μg L^{-1} [2-4]. Because of its non-regulation there is a growing concern over the health risks to humans and animals due to their persistence and accumulation in the environment.

Metronidazole (MNZ) is an antibiotic used to treat infections in humans from anaerobic bacteria and protozoa, as well as to feed additives in poultry and aquaculture farms. Its presence has been detected globally in drinking water, ground/surface water, fish-farm waters, meat industry effluents, and sewage treatment plants from 1 ng L^{-1} to 9.4 μg L^{-1} [5-8]. Due to its high polarity, low biodegradability, toxicity, potential mutagenicity and carcinogenicity [9], the removal of MNZ from water systems is crucial.

A wide range of chemical and physical technologies for antibiotics removal can be employed, for instance, chemical oxidation and biodegradation, adsorption, liquid extraction and membrane-driven techniques [10]. Among them, adsorption is one of the most commonly used because of its low cost and energy efficiency [11].

Carbon xerogels (CXs) are a novel type of adsorbent that has gained a remarkable attention due to its chemical properties and its moldable texture. CXs are nanostructured materials synthesized by the sol-gel polycondensation of resorcinol (R) and formaldehyde (F) [12] followed by curing, drying, carbonization, and activation or functionalization process, leading to carbon materials with large specific surface area (i.e. 500-1000 m^2 g^{-1}) and high porosity (ca. >80%) [13]. Few studies have been reported about the use of CXs as adsorbents of organic compounds. Zhou et al. [14] investigated the properties of CXs prepared with KOH

3

78 catalyst, and their application in dye adsorption for water treatment. They concluded that the

79 sol-gel pH value (i.e. from 6 to 9) did not show a significant influence on the surface area,

80 micropore surface area, and crystalline structure. However, the pore size was different with

81 development of mesopores at higher pH. CXs exhibited a higher adsorption capacity towards

82 both methylene blue and acid blue 40, but lower adsorption for the reactive black 5. Alvarez et

83 al. [15] investigated the removal of caffeine and diclofenac from aqueous solutions on treated

84 CXs. The maximum adsorption capacity (182.5 mg g^{-1}) was observed for adsorption of caffeine

85 onto CX treated with urea solution, due to the presence of Lewis bases on its surface, which

86 increases the adsorption affinity for organic compounds. The higher diclofenac adsorption was

87 obtained with CX treated with sulfuric acid (80.0 mg g^{-1}), mainly due to electronic interactions.

88   Graphene like species such as graphene oxide (GO) have stimulated the interest as an

89 attractive morphology-directing agent in the preparation of carbon-based materials [16]. GO

90 contains sp^2 and sp^3 hybridizations corresponding to the aromatic domain as well as to the

91 oxygenated functionalities on the graphene surface, respectively. As a result, GO has a

92 hydrophilic nature being easily dispersible in water and other polar solvents. The use of GO as

93 scaffold for carbon materials has attracted a lot of attention due to its properties such as high

94 surface area, an structure decorated with oxygen functional groups, extraordinary flexibility,

95 and accessible interface [17]. In addition, GO was already employed as cross-linked agent in

96 carbon gels from different monomers, such as resorcinol and phenol, these works being focused

97 in the development of electrodes or supercapacitors [18-19]. Tu et al. [20] synthesized graphene

98 oxide aerogel (GOA) by ice segregation induced self-assembly method to study the adsorption

99 capacity of GOA for both methylene blue (MB) and methyl orange (MO) removal. Results

100 demonstrated that GO sheets were cross-linked with each other to form GOA structure with the

101 pore size of around 50-150 μm. The maximum adsorption capacities of GOA for MB and MO

102 were 480.8 and 55.5 mg g^{-1}, respectively.

In the current work, a series of CXs were synthesized from resorcinol and formaldehyde by adding an increasing amount of a suspension of GO, and subsequently they were functionalized with urea to modify their chemical surface. CXs were chemically and texturally characterized and their performance was evaluated as adsorbent of MNZ from aqueous phase. The possible adsorption mechanism for the materials was elucidated by carrying out experiments at several solution pH, temperature, ionic strength and type of water.

2. MATERIALS AND METHODS

2.1 Chemical reagents and analytic methods

All chemical reagents used (formaldehyde, resorcinol, NaOH, graphite, $NaNO_3$, $KMNO_4$, H_2SO_4, H_2O_2 and MNZ) were analytical reagent grade supplied by Sigma-Aldrich, and were used as-received without further treatment. The deionized water used for preparation of the GO solution was obtained using Milli-Q equipment (Millipore).

The MNZ concentration in aqueous solution was analyzed by UV–visible spectrophotometry using a Shimadzu UV 1800 double-beam spectrophotometer. The absorbance of MNZ solutions was measured at a wavelength of 280 nm for a pH=2 and 320 nm for a pH from 4 to 12.

2.2 Preparation of graphene oxide (GO)

GO was synthetized from synthetic graphite (powder, particle size < 20 µm) by a modified Hummers oxidation method in which, $KMNO_4$, $NaNO_3$, and concentrated H_2SO_4 were used as reagents to prepared GO; further details are found elsewhere [21-22]. The resulting material after oxidation was dispersed in distilled water and sonicated for 1 h. Then the sonicated dispersion was centrifuged for 30 min at 4000 rpm to remove unexfoliated graphite oxide particles and a GO dispersion of 0.85 g L^{-1} was obtained.

2.3 Synthesis of GO-carbon xerogel hybrids

The carbon xerogels (CX) were synthetized using a methodology adapted from elsewhere [12, 23]. In a typical procedure, xerogels (X) were firstly prepared by dissolving the resorcinol (R) in an aqueous GO solution with different contents, which was used as solvent (W) in a glass flask under constant stirring. Then, formaldehyde (F) was added to the R-GO mixture and maintained under stirring until an uniform solution was obtained, next the pH value was adjusted to 6.5 by adding drops of 1 M solution of NaOH. After mixing, the R-F-GO mixture was transferred into 25 cm long glass tubes (0.5 cm internal diameter) and these were sealed in order to prevent evaporation. The cure process was carried out at room temperature for 1 day, 50 ℃ for 1 day and 80 ℃ for 3 days. After curing, samples were taken out from the glass tubes, cut into pellets (around 5 mm long) and soaked in acetone for 2 days to exchange the solvent media; the acetone was exchanged twice per day. The organic xerogels were placed in an oven at 110 ℃ overnight to evaporate the acetone. Finally, xerogels were carbonized under a N_2 flow of 100 mL min^{-1} at 2 ℃ min^{-1} up to 900 °C for 4 h in a horizontal tubular furnace, to finally obtain GO-CX hybrids samples. The initial GO contents in GO-CX samples were 0.62, 1.24, and 1.87 g. In addition, a CX sample without GO content for comparative purposes was also prepared by replacing the aqueous GO solution by deionized water. In all cases, the molar ratios were fixed to R/F of 0.5 and W/R of 13.6.

In a second step, GO-CX hybrids samples were functionalized with urea. Thus, 0.6 g of GO-CX hybrid finely crushed was mixed homogeneously with 0.26 g of urea, then the blend was placed inside the horizontal tubular furnace under N_2 flow (100 mL min^{-1}) at a heating rate of 2 °C min^{-1} up to 600 °C for 1 h. Functionalized GO-CX hybrids samples were labeled as CX, CX-0.3GO, CX-0.7GO and CX-1.0GO, where 0.3, 0.7 and 1.0 refers to the GO content.

2.4 Characterization studies

153   Surface morphology of functionalized GO-CX were observed by scanning electron

154   microscopy (SEM) with a Zeiss SUPRA40VP microscope equipped with a secondary electron

155   detector, backscatter electron detector and using a X-Max 50 mm energy dispersive X-ray

156   microanalysis system. Textural properties, in particular the surface area (S_{BET}), pore volume

157   (V_p) and mean pore diameter (d_p), were determined from the adsorption-desorption isotherms

158   of N_2 at 77 K using a surface area and porosimetry analyzer (Micromeritics ASAP 2020). The

159   Brunauer, Emmett and Teller (BET) and Barret, Joyner and Halenda (BJH) methods were

160   applied to calculate the S_{BET} and the pore size distribution, respectively [24, 25]. In addition, to

161   calculate the micropore volume, W_0, and mean micropore width, L_0, the Dubinin-Radushkevich

162   and Stoeckli equations were applied, respectively [26]. Lastly, the mesopore volume, V_{mes}, was

163   calculated by the difference between the amount of N_2 adsorbed at a relative pressure of 0.95

164   and W_0. X-ray photoelectron spectroscopy (XPS) analysis was performed by using a Physical

165   Electronics ESCA 5701 equipped with a MgKα X-ray source operating at 12kV and 10 mA,

166   and a hemispherical electron analyzer. The Raman spectroscopy analysis was recorded at room

167   temperature using a Micro-Raman laser spectrometer (Thermo Scientific, laser DXR 532 nm),

168   with a scanning range between 50 and 3500 cm^{-1} and at a laser power of 24 Mw. Finally, the

169   pH of point of zero charge (pH_{pzc}) was obtained by the titration acid-base method described by

170   Kuzin and Loskutov [27].

171

172   **2.5 Equilibrium adsorption experiments**

173   The adsorption capacity of all functionalized GO-CX hybrids samples towards MNZ

174   was obtained from adsorption experiments carried out in batch adsorber mode. Concisely, 40

175   mL of MNZ solution with initial concentration ranging from 100 to 600 mg L^{-1} were placed in

176   contact with a known mass of GO-CX hybrid sample into a batch adsorber. The adsorber was

177   placed in a water bath at a constant temperature. Previous experiments showed that adsorption

178 equilibrium was reached in ten days; during this period the solution pH was kept constant by

179 adding drops of 0.01 M HNO_3 or NaOH solutions as necessary.

180   The effect of pH was analyzed by obtaining the adsorption isotherms at pH 2, 5, 8 and

181 12, while the effect of temperature was carried out at 288, 298 and 308 K. Finally, the effect of

182 ionic strength was determined by adding different concentrations of NaCl, ranging from 0.01

183 to 0.5 N. In order to analyze the effect of the type of water on the adsorption capacity, the

184 adsorption isotherms were obtained under the same procedure described above but using treated

185 water from a Water Treatment Plant, located in the capital of San Luis Potosí, SLP, México.

186 The physicochemical characteristics of water were obtained by standard methods for the

187 examination of water and wastewater [28]. After equilibrium was reached, an aliquot of 5 mL

188 was taken to determine the final concentration of MNZ. The mass adsorbed of MNZ per gram

189 of GO-CX hybrids, (q), was calculated by using the following equation:

$$q = \frac{V(C_0 - C_e)}{m} \qquad (1)$$

190   where C_0 is the initial concentration of MNZ solution (mg L^{-1}), C_e is MNZ concentration

191 at equilibrium (mg L^{-1}), V is the volume of MNZ solution in the batch adsorber (L), and m is

192 the mass of GO-CX hybrid (g).

193   The experimental adsorption equilibrium data for MNZ were fitted by Sips adsorption

194 isotherm model, also known as Freundlich-Langmuir adsorption isotherm model and

195 represented by the following equation.

$$q = q_m \frac{bC_e^{(1/n)}}{1 + bC_e^{(1/n)}} \qquad (2)$$

196 Where Ce is the concentration of the solute at the equilibrium, mg L^{-1}, 1/n is a parameter related

197 to the heterogeneity adsorption, b is an equilibrium constant related to heat adsorption, L mg^{-1};

198 and q_m is the maximum adsorption capacity, mg g^{-1}. The adsorption isotherm parameters were

199 estimated by fitting the isotherm model to the experimental data using the Rosenbrock-Newton

200 algorithm as an optimization method. The quality of the fit is evaluated by calculating the

201 percentage deviation, %D for each isothermal model by the following expression:

$$\%D = \left(\frac{1}{N} \sum_{i=1}^{N} \left| \frac{q_{i,exp} - q_{i,pred}}{q_{i,exp}} \right| \right) \times 100 \ \%$$

(3)

202 where N represents the number of experiments; $q_{i,exp}$ is the experimental mass of MNZ adsorbed

203 at equilibrium, mg g^{-1}; and $q_{i,\ pred}$ is the mass of MNZ adsorbed predicted with the adsorption

204 isotherm, mg g^{-1}.

205

206 **3. RESULTS AND DISCUSSION**

207 **3.1 Textural and chemical characterization of GO-CX hybrids**

208   The textural properties of all GO-CX hybrids were analyzed by physical adsorption of

209 N$_2$ at 77 K. Fig. 1a depicts the type of isotherms for CX, CX-0.3GO, CX-0.7GO and CX-1.0GO.

210   They are a combination of Type I and IV isotherms, which are characteristic for micro

211 and mesoporous materials, respectively. In addition, a large hysteresis loop type H3 is shown

212 at relative pressures between 0.70 and 0.95 corresponding to the capillary condensation in

213 mesopores. The textural properties from adsorption isotherms for all materials are summarized

214 in Table 1. It is noteworthy, the addition of any GO dosage during the CX synthesis resulted in

215 the increase of S$_{BET}$, W$_0$ and V$_{meso}$. In fact, the CX sample (without GO loading), had the lowest

216 S$_{BET}$ and V$_{meso}$. In general, the porosity of the samples was enhanced with the addition of

217 increasing GO contents. In this way, the S$_{BET}$ of CX-0.3GO, CX-0.7GO, and CX-1.0GO

218 increased 13.8, 18.5 and 25.9 % respectively, compared to CX. Their W$_0$ values also increased

219 17.4, 33.2 and 41.6% correspondingly. Thus, CX-1.0GO sample presented the greatest S$_{BET}$

220 and larger micropore and mesopore volumes. In addition, the mean micropore size (L$_0$) was

221 also influenced by the incorporation of GO in the samples, narrower micropores being obtained

222 with larger GO contents, i.e., 1.23 and 0.91 nm for CX and CX-1.0GO, respectively

223
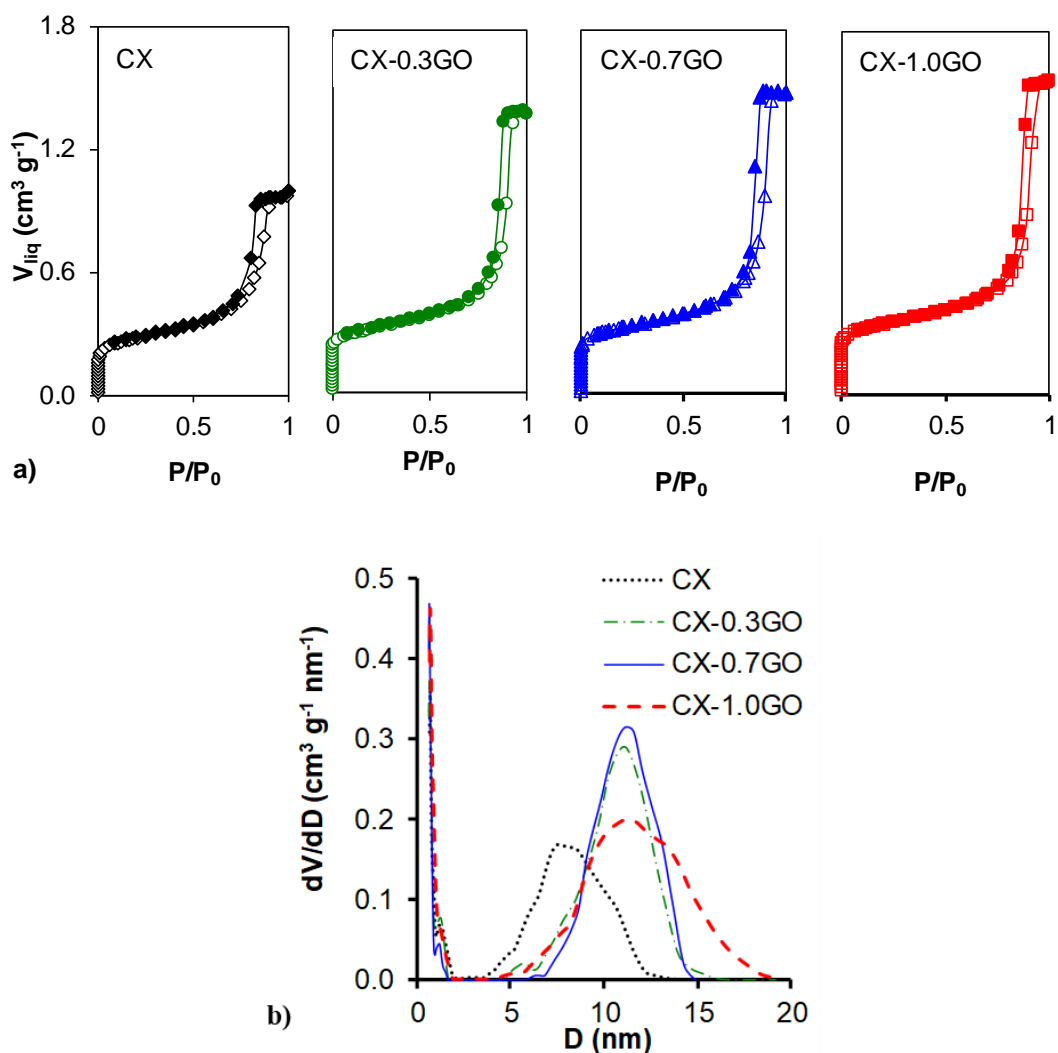
Fig. 1. (a) N_2 adsorption-desorption isotherms and (b) pore size distributions obtained by the QSDFT method applied to N_2 adsorption data for CX, CX-0.3GO, CX-0.7GO and CX-1.0GO samples.

On the other hand, the pore size distribution (PSD) calculated by QSDFT to the isotherm data for CX, CX-0.3GO, CX-0.7GO and CX-1.0GO showed the occurrence of mesopores in the range of 7-12 nm, as well as narrow micropores (Fig. 1b). The addition of any GO content during the CX synthesis modified also the mesopore size, larger mesopores of 12 nm being obtained in comparison with the CX sample. Therefore, the use of GO as cross-linked agent seems to influence on the R-F polymerization and consequently, the textural properties of the corresponding CX samples.

236

237 **Table 1.** Textural properties and pH_{PZC} of samples: CX, CX-0.3GO, CX-0.7GO, and CX-1.0GO.

Sample	S_{BET} $(m^2\,g^{-1})$	W_0 $(cm^3\,g^{-1})$	L_0 (nm)	$V_{0.95}$ $(cm^3\,g^{-1})$	V_{meso} $(cm^3\,g^{-1})$	pH_{PZC}
CX	648	0.28	1.23	0.97	0.69	8.25
CX-0.3GO	738	0.29	1.00	1.34	1.05	8.45
CX-0.7GO	768	0.29	0.95	1.44	1.15	8.42
CX-1.0GO	816	0.34	0.91	1.53	1.19	8.61

238

239

240   The morphological analysis of CX, CX0.3GO, CX-0.7GO and CX-1.0GO was studied

241 by SEM (Figs. 2a-d, respectively). In general, the morphology of all GO-CX hybrids samples

242 consists of aggregates of small spherical primary particles, which are inter-connected leading

243 to pores. This morphology is similar to that observed for other carbon xerogel materials [29,

244 30]. The nature of particles agglomeration is related with the synthesis conditions, the drying

245 as well as the carbonization process. In our case, the addition of any GO content seems to lead

246 to larger spaces between the agglomerates of primary particles, which is in agreement with the

247 results obtained from the isotherms data.

248

249

250
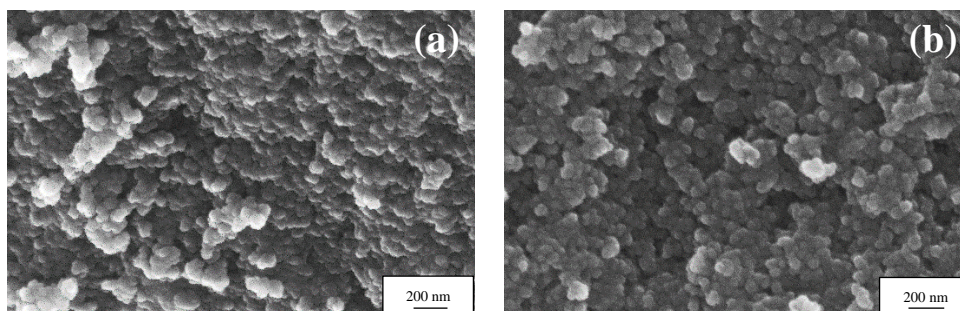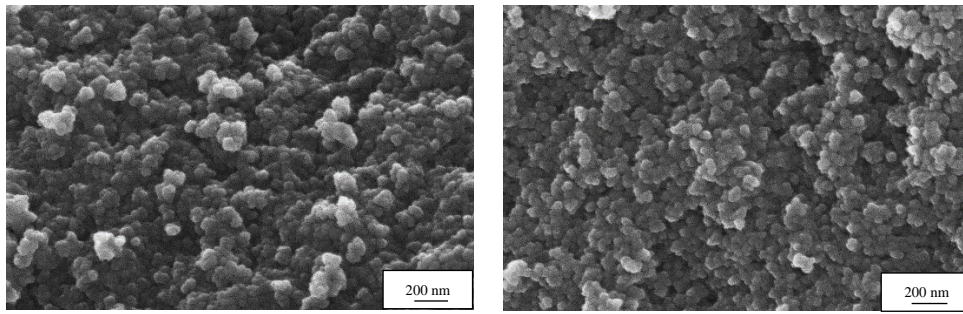
Fig. 2. SEM microphotographs of (a) CX, (b) CX-0.3GO, (c) CX-0.7GO, and (d) CX-1.0GO respectively.

Fig. 3 depicts the Raman spectra of CX, CX0.3GO, CX-0.7GO and CX1.0GO. The spectra show two characteristic peaks at ca. 1345 cm^{-1} and 1590 cm^{-1} corresponding to the D and G bands respectively. G band corresponds to sp^2-hybridized carbons and the D band corresponds to sp^3-hybridized carbons form the amorphous disordered structures [31]. Additionally, the graphitization degree of carbon materials can be evaluated by the intensity ratio of D and G bands (I_D/I_G). Thus, materials with higher graphitization degree present smaller values of I_D/I_G ratio. The I_D/I_G ratio for all GO-CX hybrids samples are also shown in Fig. 3, CX and CX-1.0GO samples show the lower and higher graphitization degree, respectively.
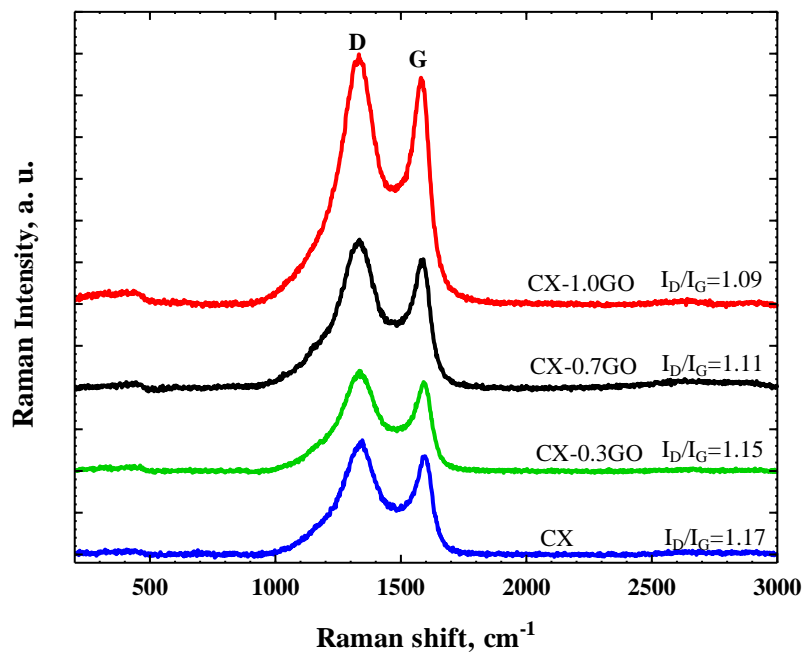
Fig. 3. Raman spectra of CX, CX-0.3GO, CX-0.7GO, and CX-1.0GO samples.

12

263

The surface chemistry of all GO-CX hybrids samples was analyzed by X-ray photoelectron spectroscopy (XPS). Fig. 4 shows the deconvoluted XPS spectra of a) C1s, b) O1s and c) N1s regions of the CX, CX-0.3GO, CX-0.7GO and CX-1.0GO samples. Table 2 shows that the carbon, oxygen, and nitrogen surface contents of GO-CX hybrids are ranging from 94.7 to 96.5, from 3.2 to 2.7, and from 2.2 to 0.8% respectively. It is noteworthy that the oxygen content decreases as the GO percentage increases, which might be attributed to the thermal reduction of the oxygen-containing groups placed in the basal planes of GO during the xerogel carbonization [31]. Analogously, the nitrogen content varied in the same way because of reactivity between urea and the oxygen functionalities.
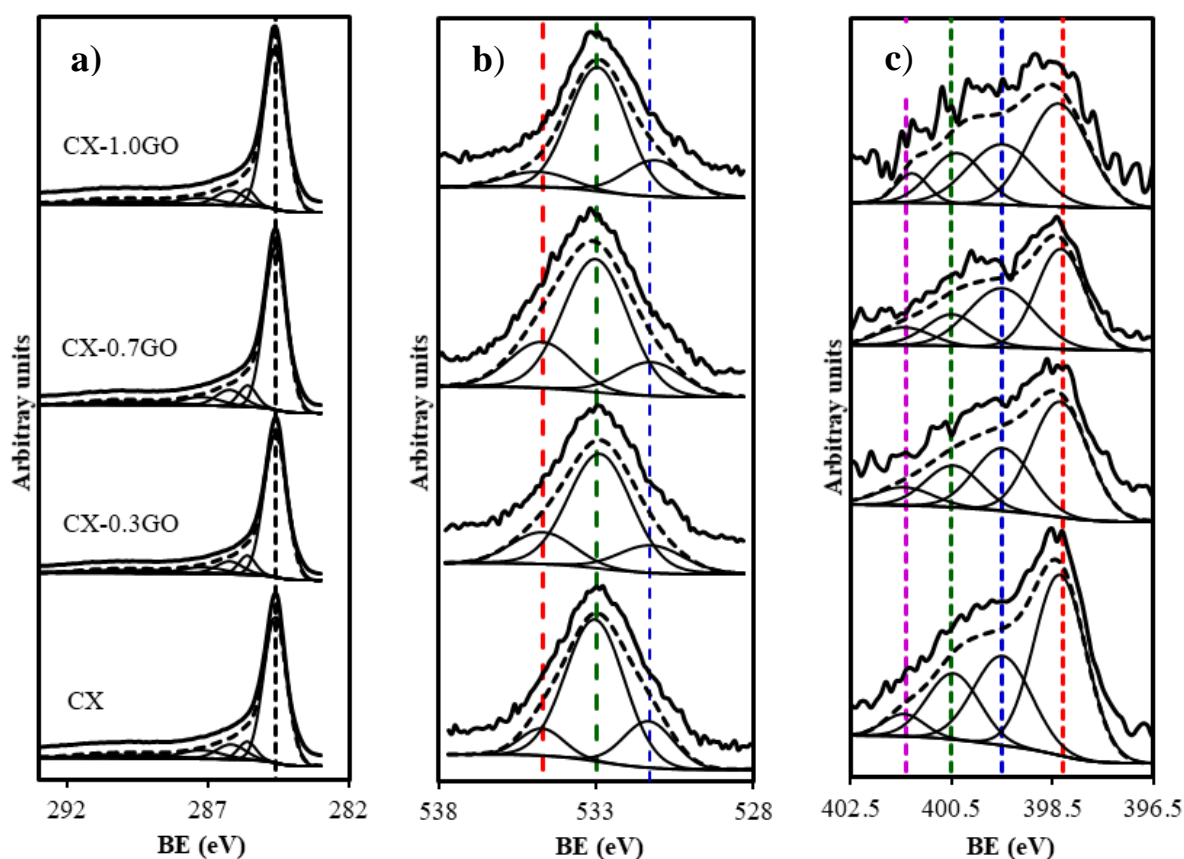
Fig. 4. XPS spectra and deconvolution of the a) C1s region, b) O1s region and c) N1s region of the CX, CX-0.3GO, CX-0.7GO and CX1.0GO samples.

As can be observed in Table 2 and Fig. 4, samples have the same C1s spectra profile, which was deconvoluted in seven peaks; at the binding energy (BE) of 284.6 eV is assigned to C=C, while the BE of 285.6 eV is attributed to C–C. The BE of 286.2 eV is associated to C–OH, whereas the BE of 287.2 eV is related to C=O. The BE of 289.1 eV is commonly attributed to COO^-, the BE of 290.3 eV is associated to CO_2, and the BE of 291.4 eV is assigned to C=O such as carbonyl, carboxylate and carboxyl groups [32]. On the other hand, the O1s spectra presents only three peaks, the first peak at the binding energy (BE) of 531.3 eV is attributed to C=O, the one at 533.0 eV is associated to anhydride, lactone, and carboxylic acids and the last peak at BE of 534.7 eV corresponds to chemisorb H_2O and /or O_2 [33]. It is important to mention that at BE of 534.7 eV the C–O and C=O groups decreased and the group –OH increased, this is probably due to the formation of C–OH groups at the edges of the graphene nanocrystals since the thermal treatment has been carried out under inert atmosphere, electrons sigma were produced being these very reactive when are in contact with air consequently fixing H_2O. Lastly, the region of N1s revealed four N–C bonds, the first bond being as pyridine type (C=N-C) at BE of 398.3 eV, the bond at BE of 399.5 eV is typically associated to NH_2, the bond at BE of 400.5 eV is attributed to N_5 or N replacing C in graphite plane and at BE of 401.4 eV is assigned to NH^+, thus the latter confirms that the functionalization with urea was efficient. Bertóti et al. [34] modified the surface of graphene and graphite by nitrogen plasma and reported similar peaks for N1s region.

Table 2. Relative surface concentration (%) of carbon, oxygen and nitrogen functionalities from the deconvolution XPS spectra for CX, CX0.3GO, CX-0.7GO, and CX-1.0GO samples.

Sample	C_{1s}	FWHM (eV)	% peak	% C	O_{1s}	% peak	% O	N_{2s}	% peak	% N
CX	284.6	0.97	69	94.7	531.3	19	3.2	398.3	50	2.2
	285.6		6		533.0	71		399.5	27	
	286.2		9		534.7	10		400.5	18	
	287.2		7					401.4	5	
	289.1		4							
	290.3		4							
	291.4		1							

|										
CX-0.3GO	284.6	0.96	70	95.3	531.3	16	3.1	398.3	49	1.6
	285.6		7		532.9	66		399.5	27	
	286.2		8		534.7	18		400.5	17	
	287.2		7					401.4	8	
	289.0		4							
	290.3		4							
	291.4		1							
CX-0.7GO	284.6	0.96	68	95.9	531.3	15	2.9	398.3	42	1.2
	285.6		7		533.0	64		399.5	33	
	286.2		8		534.7	21		400.5	15	
	287.2		7					401.4	9	
	289.0		4							
	290.3		4							
	291.3		1							
CX-1.0GO	284.6	0.96	71	96.5	531.3	26	2.7	398.3	42	0.8
	285.6		5		533.0	60		399.5	28	
	286.2		9		534.7	14		400.4	19	
	287.3		6					401.4	10	
	289.2		4							
	290.4		4							
	291.2		1							

3.2 Metronidazole adsorption equilibrium

The experimental data obtained during the adsorption equilibrium of MNZ on all adsorbents at different pH values, temperature, ion strength and type of water, were interpreted according to the isotherm model of Sips. The parameters of this model and the %D are summarized in Table 3. In this table it is evident that the isotherm yielded low value of %D indicating that it properly predicts the experimental data.

Fig. 5a shows the experimental adsorption equilibrium data of MNZ on CX, CX-0.3GO, CX-0.7GO, and CX-1.0GO where it can be observed that the mass of MNZ adsorbed depends drastically on the GO content present in the samples. The adsorption capacity increased in the following order CX < CX-0.3GO < CX-0.7GO < CX-1.0GO which is directly related to the augment of the S_{BET} of the materials due to the addition of GO. The maximum adsorption capacity of CX-1.0GO was q_m=166.46 mg/g, and it was 1.24, 1.37 and 1.51 folds greater than that obtained by the samples CX-0.7GO, CX-0.3GO and CX, respectively. Carrales-Alvarado et al. [35] investigated the adsorption mechanism of MNZ on carbon materials including activated carbon fiber, commercial activated carbon and carbon nanotubes. The authors

313   demonstrated that the mechanism governing the adsorption of MNZ is π-π dispersive

314   interactions and the presence of repulsive electrostatic forces take place only under very acidic

315   conditions. In this sense, the values of q_m for the four materials were correlated with S_{BET} in

316   Figure 5b, obtaining almost a linear relationship between S_{BET} and q_m confirming that π-π

317   interactions are responsible for the adsorption of MNZ. Moreover, CX-1.0GO sample had the

318   highest degree of graphitization which enhances the adsorption of MNZ.

319   The results displayed in Figure 5b could indicate that an increase in GO content greater

320   than 1.87 mg will lead to an increase in adsorption capacity, however it is important to note that

321   L_0 reduces gradually by increasing GO content (see Table 1), which would hinder the diffusion

322   of MNZ into the narrow micropores diminishing the adsorption capacity.

(a)

(b)
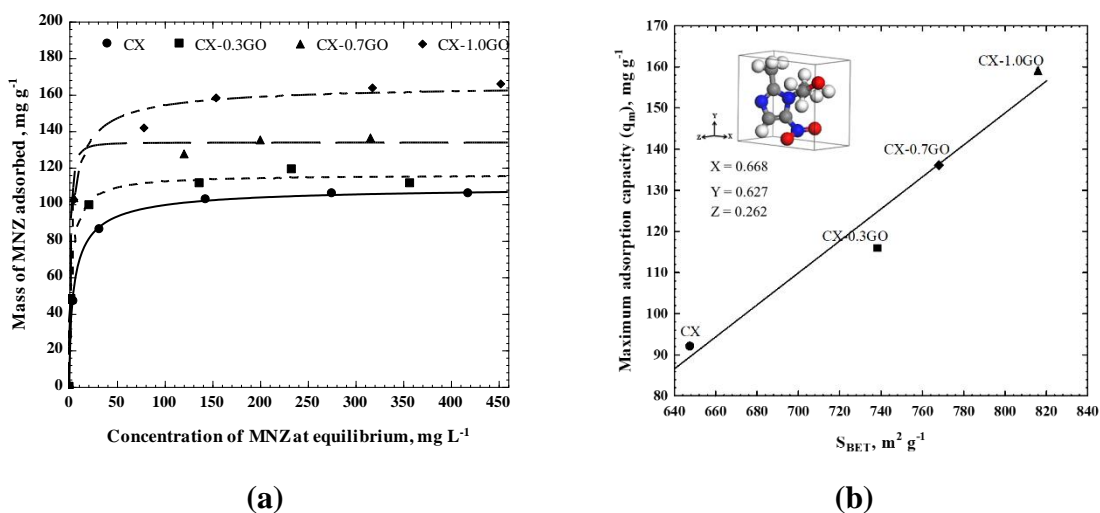
323   **Fig. 5**. (a) Adsorption isotherms of MNZ on CX, CX-0.3GO, CX-0.7GO, and CX-1.0GO at pH

324   = 5 and T = 298 K. The lines represent the prediction of Sips isotherm model. (b) Effect of the

325   S_{BET} on the adsorption capacity of CX, CX-0.3GO, CX-0.7GO, and CX-1.0GO.

326

3.2.1 Effect of solution pH

328   The solution pH is an important factor since affects significantly the surface charge of the

329   adsorbents and the MNZ species formed in the solution. The effect of solution pH was

330   investigated at pH values of 2, 5, 8, and 12. Table 3 presents the obtained constants of the

331 adsorption isotherm, while Fig. 6 summarizes the results obtained, where the q_m value of the

332 Sips isotherm was plotted *versus* the solution pH because all the isotherms presented a type L

333 behavior.
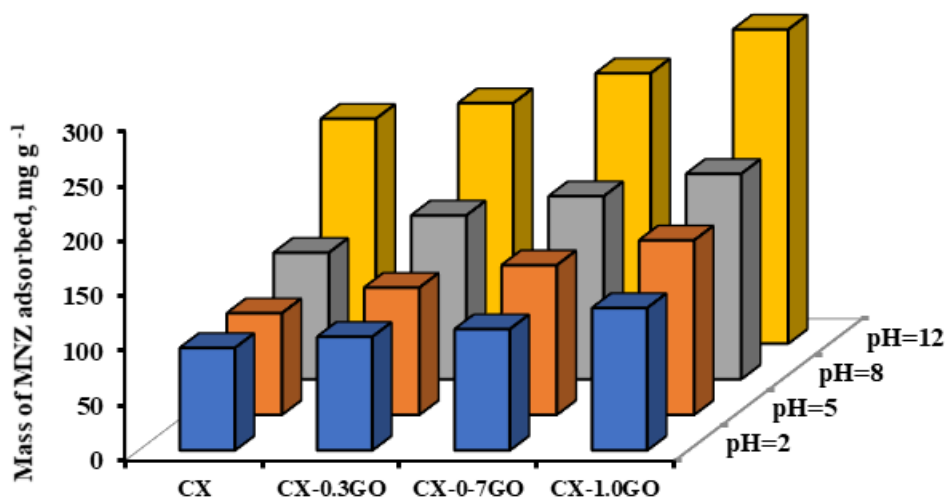
334

335 **Fig. 6.** Effect of the solution pH on the adsorption capacity of all adsorbents at T = 298 K.

336

337 The adsorption capacity increases with the initial solution pH, thus, the highest adsorption was

338 obtained at pH of 12 indicating the presence of various types of interactions during MNZ

339 adsorption (Fig. 6). According to the pK_a value of MNZ (pK_a=2.58), this molecule is almost in

340 its protonated form at pH $\leq$ 2 and in a zwitterion form at pH $\geq$ 4 [35]. Furthermore, based on

341 the similar pH_{PZC} values of adsorbents, their surface charge is positive at pH $<$ pH_{PZC} and

342 negative at pH $>$ pH_{PZC}. Thus, at pH $=$ 2 the lowest MNZ adsorption capacity can be attributed

343 to the establishment of repulsive electrostatic interactions between the materials surface and the

344 cationic species of MNZ, although it is important to emphasize that even under these conditions

345 the adsorption capacity of the CXs is considerably high (94.2 mg g^{-1}), which is due to the π-π

346 dispersive interactions.

347

348

349

350

351

352

Table 3. Values of the parameters for Sips (Freundlich-Langmuir) adsorption isotherms and average absolute percentage deviations (%D).

Sample	Effect	Sips isotherm parameters			
		q_m (mg g^{-1})	b	n	%D
CX	pH=2	94.25	0.02	0.84	2.25
	pH=5	110.15	0.27	1.3	0.78
	pH=8	142.27	0.48	2.8	0.93
	pH=12	224.95	0.37	1.97	3.81
	288 K	97.47	0.75	2.07	3.93
	298 K	91.72	0.02	0.32	3.83
	308 K	116.86	0.02	0.65	3.36
	Deionized water	100.12	0.29	1.01	11.96
	Treated water	88.44	1.03	1.03	10.57
CX-0.3GO	pH=2	116.08	0.35	1.04	1.25
	pH=5	121.19	0.01	0.68	1.83
	pH=8	167.08	0.23	1.76	0.13
	pH=12	241.23	0.09	1.47	6.57
	288 K	105.85	0.09	0.98	2.46
	298 K	121.19	0.01	0.68	1.83
	308 K	126.04	0.14	1.79	3.61
	Deionized water	118.79	0.41	1.2	12.60
	Treated water	108.16	0.76	0.98	13.42
CX-0.7GO	pH=2	148.79	0.21	2.25	3.07
	pH=5	133.59	0.36	0.61	1.63
	pH=8	176.04	0.21	1.44	4.04
	pH=12	257.33	0.12	1.3	7.03
	288 K	130.48	0.17	0.95	1.49
	298 K	133.59	0.36	0.61	1.63
	308 K	148.69	0.04	0.99	5.58
	Deionized water	137.03	0.6	1.2	8.27
	Treated water	123.52	0.66	0.9	2.24
CX-1.0GO	pH=2	140.18	0.22	1.46	2.09
	pH=5	166.44	0.44	1.38	4.49
	pH=8	218.89	0.35	2.10	0.92
	pH=12	278.34	0.10	1.31	4.34
	288 K	148.31	0.15	0.98	3.17
	298 K	162.06	0.39	1.02	4.21

308 K	172.59	0.20	0.99	7.57
Deionized water	152.64	0.73	1.10	8.39
Treated water	146.8	0.99	1.3	7.75

355

356 On the other hand, at pH=5 and 8 the adsorption capacity increased, this can be related to a

357 different mechanism since at these pH values, the MNZ specie is in a zwitterion form and the

358 surface charge is positive, thus attractive electrostatic interactions between the O^- of MNZ and

359 the surface of CXs can be promoted. Additionally, hydrogen bonds might be formed between

360 the $-NO_2$ group in the MNZ molecule and $-NH_2$ groups (from the functionalization with urea),

361 in this sense, $-NO_2$ group is acting as the H-acceptor and $-NH_2$ group as the H-donor [36], and

362 dispersive interactions are established between π-π electrons of the aromatic ring of the MNZ

363 molecule and the π electrons of the graphene planes of the GO-CX hybrids. Similar results have

364 been reported by Rivera-Utrilla et al. [37] and Carrales-Alvarado et al. [35]. Lastly, the

365 noticeable increase of MNZ adsorption at pH=12 might be due to hydrophobic and π-π

366 dispersive interactions, Carrales-Alvarado et al. [35] stated that at pH=12 the solubility of MNZ

367 is reduced because of the high electrolyte concentration, augmenting the interactions between

368 the hydrophobic activated carbon surface sites and MNZ molecules, then increasing the MNZ
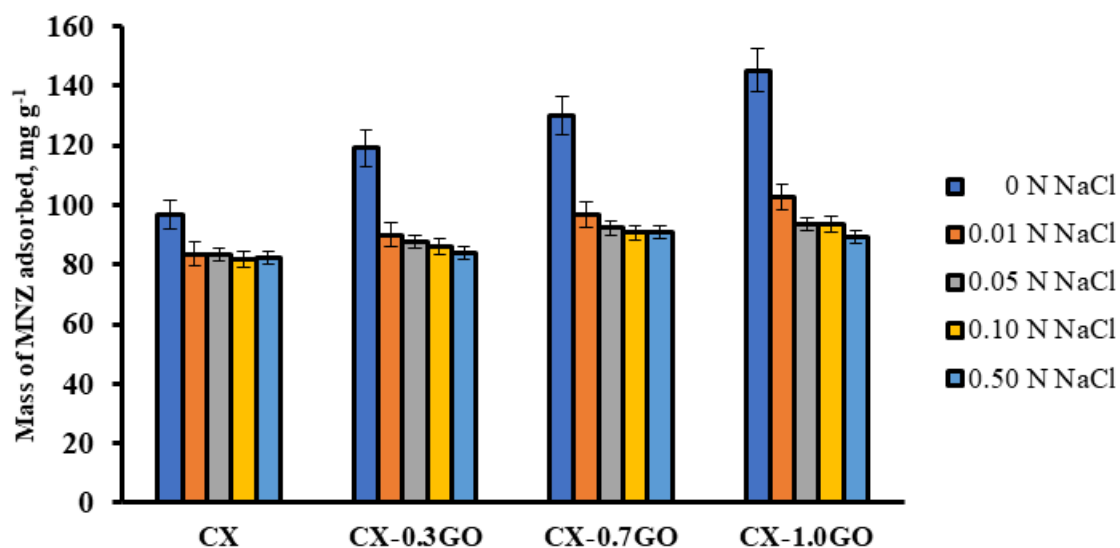
369 adsorption.

370

371 **3.2.2 Effect of ionic strength, temperature and type of water**

372 The effect of ionic strength was carried out in the presence of increasing NaCl concentrations,

373 ranging from 0.01 to 0.5 N, at T = 298 K and without controlling pH. The initial solution pH

374 was in the range of 4.21 to 5.02, respectively. Thereafter, once the experiments attained

375 equilibrium, the final solution pHs were in the range of 5.9 to 7.2. Fig. 7 depicts the effect of

376 ionic strength on the adsorption capacity of CX, CX-0.3GO, CX-0.7GO, and CX-1.0GO

377 towards MNZ. The parameters of the adsorption isotherms model are shown in Table 3. As it

378 can be observed in Fig. 7, in general, there is a noticeable effect of ionic strength at low NaCl

379 concentration (0.01 N). In fact, the effect at this concentration, is even more evident for CX-

380   1.0GO sample, since the adsorption capacities of CX, CX-0.3GO, CX-0.7GO, and CX-1.0GO

381   towards MNZ were reduced, 1.16, 1.32, 1.34, and 1.41 times fold, respectively. This might be

382   attributed to the fact that chemical interactions are established between the high content of

383   surface functional groups present on CX-1.0GO and Na ions, thus impeding MNZ molecules

384   from be adsorbed. Moreover, it is observed that above 0.01 to 0.5 N NaCl, the adsorption

385   capacities of CX, CX-0.3GO, CX-0.7GO, and CX-1.0GO remained almost constant. Some

386   researchers have also studied the effect of ionic strength, for instance Ocampo-Pérez et al. [38]

387   investigated the effect of ionic strength from 0.01 to 1.0 M of NaCl. Their results revealed that

388   the presence of NaCl favored the MNZ adsorption onto activated carbon cloth, this behavior

389   was explained by the solubility decrease due to the increasing of ionic strength. On the contrary,

390   Carrales-Alvarado et al. [35] and Rivera-Utrilla et al. [37] reported that the MNZ adsorption

391   onto different activated carbons was not affected by the increase of ionic strength which proved

392   that in these cases the adsorption process is not governed by electrostatic interactions.

393

394   **Fig. 7**. Effect of solution ionic strength on the MNZ adsorption capacity of CX, CX-0.3GO,

395   CX-0.7GO, and CX1.0GO at T = 298 K.

396

397   The influence of temperature on MNZ adsorption onto GO-CX hybrids samples was

398   investigated at 288, 298, and 308 K and pH 5. Fig. 8 depicts the adsorption isotherms of MNZ

399   onto CX, CX-0.3GO, CX-0.7GO, and CX-1.0GO. In general, the MNZ adsorption shows a

400   slightly increase as the temperature is elevated from 288 to 298 K and from 298 to 308 K. The

401   temperature increase causes an increase in kinetic energy. Thus, the higher kinetic energy

402   causes more motion in the MNZ molecules favoring its adsorption, so it can be inferred that the

403   adsorption process in this case was endothermic.
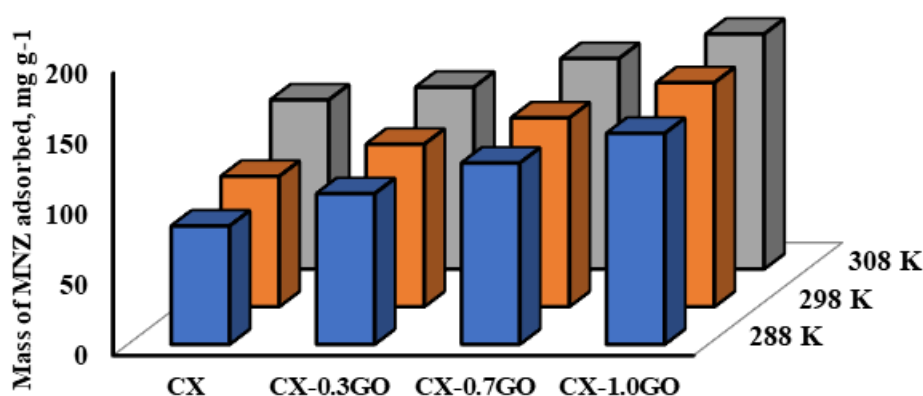
404

405   **Fig. 8.** Effect of temperature on the MNZ adsorption capacity of CX, CX-0.3GO, CX-0.7GO,

406   and CX-1.0GO at 288, 298, and 308 K and pH = 5.

407

408   The effect of type of water on the MNZ adsorption capacity over GO-CX hybrids

409   samples was also studied using treated water to prepare the MNZ solution. Table 4 summarized

410   the results obtained from the physicochemical analysis of treated water used. These results show

411   that treated water has a neutral pH and low content of different ions. Fig. 9 depicts the

412   adsorption isotherms of MNZ onto CX, CX-0.3GO, CX-0.7GO, and CX-1.0GO samples using

413   deionized and treated water. The values of the isotherm parameters as well as the average

414   absolute percentage deviation are gathered in Table 3.

415

416

417
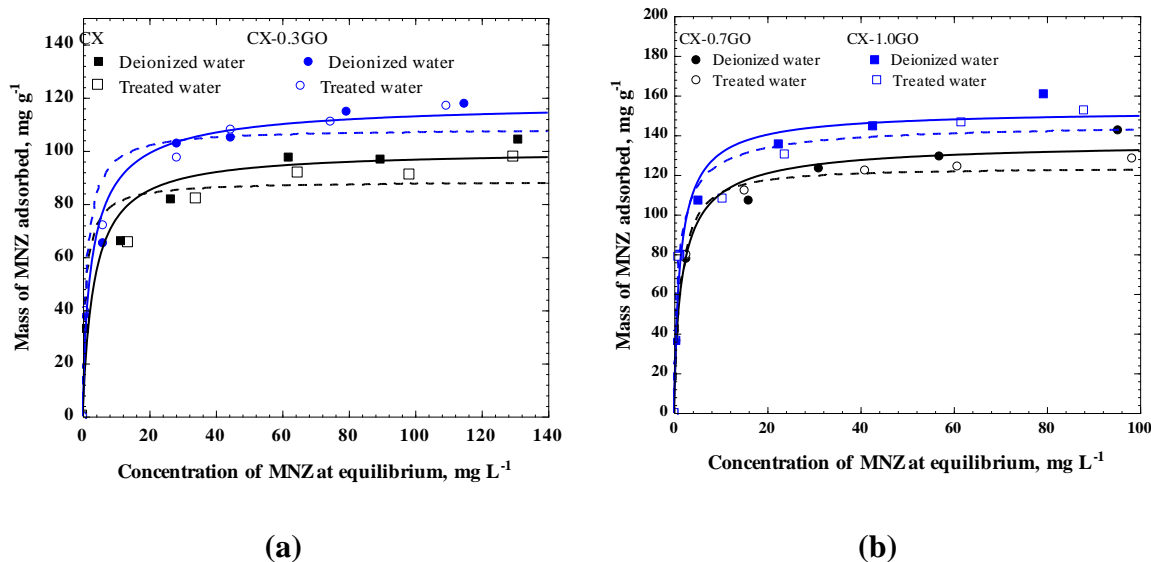
Fig. 9. Adsorption isotherms of MNZ on (a) CX and CX-0.3GO, and (b) CX-0.7GO, and CX-1.0GO at pH=5 and 298 K. The lines represent the prediction of Sips isotherm model. Effect of treated water.

421

As seen in Fig. 9, results exhibit a negligible decrease of the mass of MNZ adsorbed on GO-CX hybrids samples using treated water despite of the presence of several ions, which means MNZ molecules and ions in treated water were adsorbed by different mechanisms without inhibiting the MNZ adsorption. As stated previously, the MNZ adsorption is mainly governed by π-π dispersion interactions between the aromatic ring of MNZ molecule and the graphene layers of GO-CX hybrids. Additionally, this effect could be also related with the low concentration of ions (i.e. nitrates, carbonates, sulfates, or chlorides) in this type of water (Table 4). Carrales-Alvarado et al. [35] also studied the effect of wastewater on the MNZ adsorption onto different types of carbons, their results shown that the presence of ions caused a synergistic effect thus increasing the MNZ adsorption instead of competing with the ions.

434 **Table 4.** Physicochemical properties of treated water.

Parameter	Value	Parameter	Value
pH	6.91	Phosphates dissolved (mg PO L^{-1})	No detected
Alkalinity (mg $CaCO_3$ L^{-1})	20	Fluoride (mg L^{-1})	0.47
Bicarbonates (mg $CaCO_3$ L^{-1})	20	Nitrites (mg L^{-1})	No detected
Calcium (mg L^{-1})	6.4	Nitrates (mg L^{-1})	4
Chlorides (mg L^{-1})	10	Magnesium (mg L^{-1})	2.59
Total hardness (mg $CaCO_3$ L^{-1})	25	Silice (mg SiO_2 L^{-1})	18
Calcium hardness (mg $CaCO_3$ L^{-1})	16	Total dissolved solids (TDS) (mg L^{-1})	98
Magnesium hardness (mg $CaCO_3$ L^{-1})	9	Sulfates (mg L^{-1})	36

435

436

437 **CONCLUSIONS**

438 The use of GO as cross-linked agent seems to influence on the R-F polymerization and

439 consequently, the textural properties of the corresponding CX samples. CX-1.0GO sample

440 presented the greatest surface area and larger micropore and mesopore volumes.

441 According to Raman spectroscopy, the sample CX-1.0GO showed the higher

442 graphitization degree. XPS results revealed that the oxygen content decreases as the GO

443 percentage increases, which might be attributed to the thermal reduction, in the same way

444 nitrogen content decreases because of reactivity among urea and the oxygen functionalities.

445 The adsorption of MNZ onto GO-CX hybrids is governed by different mechanisms that

446 includes π-π dispersive interactions between the graphene planes of GO-CX hybrids and the

447 aromatic ring of MNZ molecule, attractive electrostatic interactions (at pH=8) and by hydrogen

448 bonding.

449 The MNZ adsorption process was endothermic nature. At low ionic strength (0.01 N

450 NaCl) the mass of MNZ adsorbed decreased but above this concentration remained almost

451   constant. Additionally, the presence of different cations and ions at low concentrations in

452   wastewater, did not affect the MNZ adsorption. These advanced materials show potential to be

453   used as adsorbents in environmental applications.

454

464 **REFERENCES**

465 [1]   Nisha, A. R. (2008). Antibiotic residues-a global health hazard. Vet. World, *1*(12), 375.

466 [2]   Le Page, G., Gunnarsson, L., Snape, J., Tyler, C. R. (2017). Integrating human and

467   environmental health in antibiotic risk assessment: a critical analysis of protection goals,

468   species sensitivity and antimicrobial resistance. Environ. Int., 109, 155-169.

469 [3]   Laffite, A., Kilunga, P. I., Kayembe, J. M., Devarajan, N., Mulaji, C. K., Giuliani, G.,

470   Poté, J. (2016). Hospital effluents are one of several sources of metal, antibiotic resistance

471   genes, and bacterial markers disseminated in Sub-Saharan urban rivers. Front.

472   Microbiol., 7, 1128.

473 [4]   Uchida, K., Konishi, Y., Harada, K., Okihashi, M., Yamaguchi, T., Do, M.H., et al., 2016.

474   Monitoring of antibiotic residues in aquatic products in urban and rural areas of Vietnam.

475   J. Agric. Food Chem. 64 (31), 6133–6138.

476 [5]   Leung, H. W., Jin, L., Wei, S., Tsui, M. M. P., Zhou, B., Jiao, L., Lam, P. K. S. (2013).

477   Pharmaceuticals in tap water: human health risk assessment and proposed monitoring

478   framework in China. Environ. Health Persp., 121(7), 839-846.

479 [6]   Mahugo-Santana, C., Sosa-Ferrera, Z., Torres-Padrón, M. E., Santana-Rodríguez, J. J.

480   (2010). Analytical methodologies for the determination of nitroimidazole residues in

481   biological and environmental liquid samples: a review. Anal. Chim. Acta, 665(2), 113-

482   122.

483 [7]   Ahmadzadeh, S., Dolatabadi, M. (2018). Electrochemical treatment of pharmaceutical

484   wastewater through electrosynthesis of iron hydroxides for practical removal of

485   metronidazole. Chemosphere, 212, 533-539.

486 [8]   Gómez, M. J., Malato, O., Ferrer, I., Agüera, A., Fernández-Alba, A. R. (2007). Solid-

487   phase extraction followed by liquid chromatography–time-of-flight–mass spectrometry

488   to evaluate pharmaceuticals in effluents. A pilot monitoring study. J. Environ. Mon., 9(7),

489   718-729

490 [9] Bendesky, A., Menéndez, D., Ostrosky-Wegman, P. (2002). Is metronidazole

491 carcinogenic. Mutat. Res./Rev. Mutat., 511(2), 133-144.

492 [10] Homem, V., Santos, L. (2011). Degradation and removal methods of antibiotics from

493 aqueous matrices–a review. J. Environ. Manage., 92(10), 2304-2347.

494 [11] Sekulic, M. T., Boskovic, N., Slavkovic, A., Garunovic, J., Kolakovic, S., Pap, S. (2019).

495 Surface functionalised adsorbent for emerging pharmaceutical removal: Adsorption

496 performance and mechanisms. Process Saf. Environ., 125, 50-63

497 [12] Pekala, R. W., Alviso, C. T., Kong, F. M., Hulsey, S. S. (1992). Aerogels derived from

498 multifunctional organic monomers. *Journal of Non-Crystalline Solids*, *145*, 90-98.

499 [13] Pekala, R. W., Schaefer, D. W. (1993). Structure of organic aerogels. 1. Morphology and

500 scaling. Macromolecules, 26(20), 5487-5493.

501 [14] Zhou, G., Tian, H., Sun, H., Wang, S., Buckley, C. E. (2011). Synthesis of carbon xerogels

502 at varying sol–gel pHs, dye adsorption and chemical regeneration. Chem. Eng. J., 171(3),

503 1399-1405.

504 [15] Álvarez, S., Ribeiro, R. S., Gomes, H. T., Sotelo, J. L., García, J. (2015). Synthesis of

505 carbon xerogels and their application in adsorption studies of caffeine and diclofenac as

506 emerging contaminants. Chem. Eng. Res. Des., 95, 229-238.

507 [16] Martín-Jimeno, F. J., Suárez-García, F., Paredes, J. I., Martínez-Alonso, A., Tascón, J. M.

508 D. (2015). Activated carbon xerogels with a cellular morphology derived from

509 hydrothermally carbonized glucose-graphene oxide hybrids and their performance

510 towards CO2 and dye adsorption. Carbon, 81, 137-147.

511 [17] Xie, A., Dai, J., Cui, J., Lang, J., Wei, M., Dai, X., Yan, Y. (2017). Novel graphene oxide–

512 confined nanospace directed synthesis of glucose-based porous carbon nanosheets with

513 enhanced adsorption performance. ACS Sustain. Chem. Eng., 5(12), 11566-11576.

514 [18] Liu, L., Yang, J., Meng, Q. (2013). The preparation and characterization graphene-cross-

515   linked phenol–formaldehyde hybrid carbon xerogels. J. Sol-Gel Sci. Techn., 67(2), 304-

516   311.

517 [19] Canal-Rodríguez, M., Arenillas, A., Rey-Raap, N., Ramos-Fernández, G., Martín-Gullón,

518   I., Menéndez, J. A. (2017). Graphene-doped carbon xerogel combining high electrical

519   conductivity and surface area for optimized aqueous supercapacitors. Carbon, 118, 291-

520   298.

521 [20] Tu, T. H., Cam, P. T. N., Phong, M. T., Nam, H. M., Hieu, N. H. (2019). Synthesis and

522   application of graphene oxide aerogel as an adsorbent for removal of dyes from

523   water. Mater. Lett., 238, 134-137.

524 [21] Hummers Jr, W. S., Offeman, R. E. (1958). Preparation of graphitic oxide. J. Am. Chem.

525   Soc., 80(6), 1339-1339.

526 [22] Pastrana-Martínez, L. M., Morales-Torres, S., Likodimos, V., Figueiredo, J. L., Faria, J.

527   L., Falaras, P., Silva, A. M. (2012). Advanced nanostructured photocatalysts based on

528   reduced graphene oxide–TiO2 composites for degradation of diphenhydramine

529   pharmaceutical and methyl orange dye. Appl. Catal. B Environ., 123, 241-256.

530 [23] Morales-Torres, S., Maldonado-Hódar, F. J., Pérez-Cadenas, A. F., Carrasco-Marín, F.

531   (2010). Textural and mechanical characteristics of carbon aerogels synthesized by

532   polymerization of resorcinol and formaldehyde using alkali carbonates as basification

533   agents. Phys Chem. Chem. Phys., 12(35), 10365-10372.

534 [24] Brunauer, S., Deming, L. S., Deming, W. E., Teller, E. (1940). On a theory of the van der

535   Waals adsorption of gases. *Journal of the American Chemical society*, *62*(7), 1723-1732.

536 [25] Barrett, E. P., Joyner, L. G., Halenda, P. P. (1951). The determination of pore volume and

537   area distributions in porous substances. I. Computations from nitrogen isotherms. J. Am.

538   Chem. Soc., *73*(1), 373-380.

539 [26] Bansal, R. C., Donnet, J. B., Stoeckli, F. (1988). Active carbon.

540 [27] Kuzin, I. A., Loskutov, A. I., (1996). J. Appl. Chem. USSR 39 85.

541 [28] Baird, R. B., Eaton, A. D., Clesceri, L. S. (2012). Standard methods for the examination

542   of water and wastewater (Vol. 10). E. W. Rice (Ed.). Washington, DC: American Public

543   Health Association.

544 [29] Pérez-Cadenas, M., Moreno-Castilla, C., Carrasco-Marín, F., Pérez-Cadenas, A. F.

545   (2008). Surface chemistry, porous texture, and morphology of N-doped carbon

546   xerogels. Langmuir, 25(1), 466-470.

547 [30] Maldonado-Hódar, F. J., Moreno-Castilla, C., Pérez-Cadenas, A. F. (2004). Surface

548   morphology, metal dispersion, and pore texture of transition metal-doped monolithic

549   carbon aerogels and steam-activated derivatives. Micropor Mesopor Mat., 69(1-2), 119-

550   125.

551 [31] Pastrana-Martínez, L. M., Morales-Torres, S., Likodimos, V., Falaras, P., Figueiredo, J.

552   L., Faria, J. L., Silva, A. M. (2014). Role of oxygen functionalities on the synthesis of

553   photocatalytically active graphene–TiO_2 composites. Appl. Catal. B Environ., 158, 329-

554   340.

555 [32] Luo, D., Zhang, G., Liu, J., Sun, X. (2011). Evaluation criteria for reduced graphene

556   oxide. J. Phys. Chem. C, 115(23), 11327-11335.

557 [33] Rivera-Utrilla, J.,Sánchez-Polo, M. (2002). The role of dispersive and electrostatic

558   interactions in the aqueous phase adsorption of naphthalenesulphonic acids on ozone-

559   treated activated carbons. Carbon, 40(14), 2685-2691.

560 [34] Bertóti, I., Mohai, M., László, K. (2015). Surface modification of graphene and graphite

561   by nitrogen plasma: Determination of chemical state alterations and assignments by

562   quantitative X-ray photoelectron spectroscopy. Carbon, 84, 185-196.

563 [35] Carrales-Alvarado, D. H., Ocampo-Pérez, R., Leyva-Ramos, R., Rivera-Utrilla, J. (2014).

564   Removal of the antibiotic metronidazole by adsorption on various carbon materials from

565   aqueous phase. J. Colloid Interf. Sci., 436, 276-285.

566   [36] Seo, P. W., Khan, N. A., Jhung, S. H. (2017). Removal of nitroimidazole antibiotics from

567   water by adsorption over metal–organic frameworks modified with urea or

568   melamine. Chem. Engin. J., 315, 92-100.

569   [37] Rivera-Utrilla, J., Prados-Joya, G., Sánchez-Polo, M., Ferro-García, M. A., Bautista-

570   Toledo, I. (2009). Removal of nitroimidazole antibiotics from aqueous solution by

571   adsorption/bioadsorption on activated carbon. J. Hazar. Mater., 170(1), 298-305.

572   [38] Ocampo-Pérez, R., Orellana-Garcia, F., Sánchez-Polo, M., Rivera-Utrilla, J., Velo-Gala,

573   I., López-Ramón, M. V., Alvarez-Merino, M. A. (2013). Nitroimidazoles adsorption on

574   activated carbon cloth from aqueous solution. J. Colloid Interf. Sci., 401, 116-124.

575

576

577

578

579